Fluid displacement by Stokes flow past a spherical droplet

I. EAMES, D. GOBBY and S. B. DALZIEL

Journal of Fluid Mechanics / Volume 485 / May 2003, pp 67 - 85
DOI: 10.1017/S0022112003004361, Published online: 24 June 2003

J. Fluid Mech. (2003), *vol.* 485, *pp.* 67–85.
DOI: 10.1017/S0022112003004361 Printed in the United Kingdom

Fluid displacement by Stokes flow past a spherical droplet

By I. EAMES[1], D. GOBBY[2] AND S. B. DALZIEL[3]

[1]Departments of Mechanical Engineering and Mathematics, University College London, Torrington Place, London WC1E 7JE, UK

[2]Department of Chemical Engineering, University College London, Torrington Place, London WC1E 7JE, UK

[3]Department of Applied Mathematics and Theoretical Physics, Cambridge University, Centre for Mathematical Sciences, Wilberforce Road, Cambridge CB3 0WA, UK

(Received 3 September 2002 and in revised form 11 January 2003)

The concept of 'drift', which has been exploited in many high Reynolds number and inviscid flow problems, is here applied to examine transport by a spherical viscous droplet (of radius a) moving in a Stokes flow.

In an unbounded flow, the velocity in the direction of translation of a spherical droplet is positive everywhere because streamlines, in the fluid frame of reference, 'close' at infinity. Fluid particles are displaced a positive distance, X, forward, which is expressed in terms of the initial distance from the stagnation streamline ρ_0. Asymptotic expressions are developed for X in the limits of $\rho_0/a \ll 1$ and $\gg 1$. The nature of the singularity of the centreline displacement changes from $O(-a\log(\rho_0/a))$ to $O(a^2/\rho_0)$ as the viscosity of the droplet, compared to the ambient fluid, increases. By employing a mass-conservation argument, asymptotic expressions are calculated for the partial drift volume, D_p, associated with a circular material surface of radius ρ_m which starts far in front of a droplet that translates a finite distance. Since the velocity perturbation decays slowly with distance from the droplet, D_p tends to become unbounded as ρ_m increases, in contrast to inviscid flows.

The presence of a rigid wall ensures that the velocity perturbation decays sufficiently rapidly that fluid particles, which do not lie on the stagnation streamline, are displaced a finite distance away from the wall. The distortion of a material surface lying a distance h_L above a wall, by the droplet, starting a distance h_S from the wall and moving away, is studied. The volume transported away from the wall, calculated using a multipolar flow approximation, is $D_p = \pi h_L^2 a(3\lambda+2)/(\lambda+1)$, and is weakly dependent on the starting position of the droplet, in accordance with numerical results. When the material surface is close to the wall ($h_L/a \ll 1$), the volume transported away from a wall is significantly smaller than for inviscid flows because the no-slip condition on the rigid wall tends to inhibit 'scouring'. When the material surface is far from the wall ($h_L/a \gg 1$), the viscously dominated flow transports a larger volume of fluid away from the wall because the flow decays slowly with distance from the droplet.

These results can be generalized to arbitrarily shaped bodies, since the transport processes are dominated by the strength of the Stokeslet. The effect of boundaries and inertia on fluid transport processes is briefly discussed.

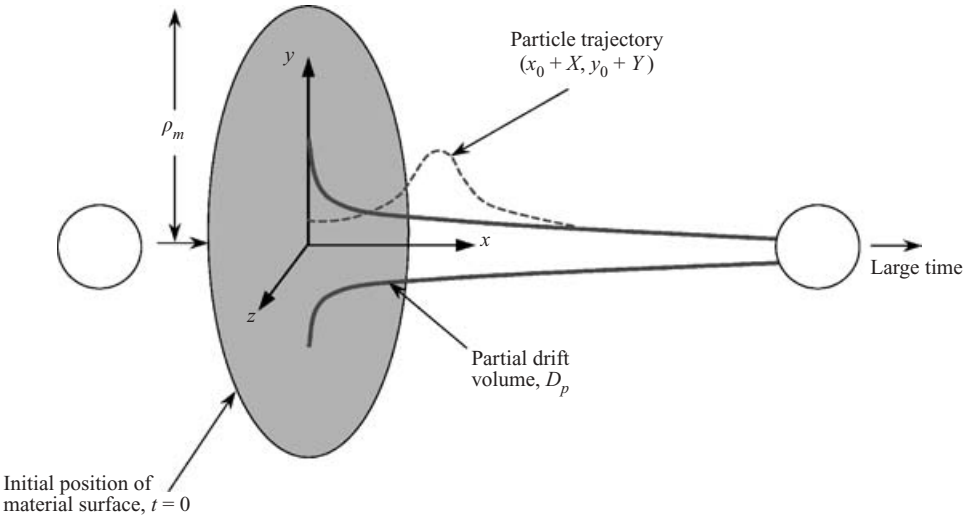

FIGURE 1. Schematic showing the deformation of a material surface by a translating body. The fluid particle trajectories indicated conform to the case of unbounded viscous flows, where there is no reflux component.

1. Introduction

Bubbles, particles and vortices moving near boundaries (such as a rigid wall or free surface) enhance heat and mass transfer processes. For instance during pool boiling, vapour bubbles grow at nucleation sites on heating elements and detach when the buoyancy force exceeds the surface tension force keeping the bubbles pinned. As vapour bubbles rise they transport a proportion of the thermal boundary layer into the colder ambient fluid, which significantly enhances the heat transfer coefficient (Forster & Greif 1959). In the context of sediment transport, saltating sand particles hopping along the surface of a soil resuspend dust through a mixture of hydrodynamic and ballistic mechanisms (Eames & Dalziel 2000). As the sand particles move away from the rigid boundary, they transport resuspended dust particles in their wake away from the wall (Owen 1980).

In order to quantify the ability of bodies to permanently transport fluid from one place to another, Darwin (1953) developed, for potential flows, the concept of the drift volume. Darwin (1953) considered how a body moving in a straight line in an unbounded flow permanently deforms a material surface, which is initially far in front of the body (see figure 1). Darwin defined the drift volume, D, to be the volume formed between the initial and final position of the material surface. In the limit of the body starting infinitely far from the surface and moving off to infinity, the drift volume is $D = C_m V$, where V is the volume of the body and C_m is the added mass coefficient. The added mass coefficient is a function of the body geometry and takes a value of 1 for a cylinder and $\frac{1}{2}$ for a sphere. There are a number of subtle mathematical qualifiers for Darwin's result to be valid, which are discussed by Benjamin (1986) and Eames, Belcher & Hunt (1994).

When a potential flow is bounded by vertical walls, the continuity ensures that there is a return flow or reflux. The deformation of a material surface initially spanning the channel, by a translating body, consists of two distinct components: a localized drift (positive displacement) component where the body passes, and a non-local reflux (negative displacement) component. The return flow or reflux created by

rising bubbles is chiefly responsible for the hindered rise speed of bubbles and the slip velocity between the gas and liquid phases (Kowe *et al.* 1988). Bush & Eames (1998) examined the fluid transport by 'planar' high Reynolds number bubbles rising in a Hele-Shaw cell, and observed good agreement between measured and predicted drift volumes. Further, an experimental study of the fluid transported by two-dimensional dipolar vortices (moving in a rotating tank) by Eames & Flor (1998) showed good agreement between measurements of the drift volume and Darwin's (1953) prediction. These experiments underline the practical significance of estimating drift volumes.

In the experimental studies described above, the influence of shed (or wake) vorticity is negligible because it is rapidly dissipated between the channel walls in the Hele-Shaw configuration, or is entrained by the vortex. In both examples, wake vorticity is also dramatically reduced by the significant straining motion near the rear stagnation point (Hunt & Eames 2002), so that the downstream flow is essentially irrotational. However, in general, wake vorticity has a significant impact on the displacement field because it sets up a finite volume flux Q downwind of the body. When the Reynolds number of the wake is large, the volume flux associated with the velocity deficit is related to F_D, the drag force on the body, through $Q = F_D/\rho_d U$ (Betz 1925), where ρ_d is the fluid density and U the flow speed. Thus the drift volume associated with trailing vorticity or downwind velocity increases with downwind distance, and Darwin's result is no longer valid. The impact of vorticity on the displacement field and drift volume has been studied in relatively few cases. Griffith (1986) studied numerically the deformation of material surfaces by a viscous thermal rising in an unbounded flow, and found that the volume displaced forward was infinite.

In addition to providing a means of quantifying the drift volume or mass flux associated with translating bodies, studying the displacement of fluid particles and material surfaces enables a Lagrangian coordinate system or framework to be developed. Such a framework permits a physical understanding and closed-form expressions for nonlinear problems – particularly high Reynolds number flows – such as the rapid distortion of turbulence (Hunt 1973) and in multiphase flows (see the review by Magnaudet & Eames 2000), where the distortion of vortical elements is related to the distortion of fluid lines/surfaces through Cauchy's result.

One reason this technique has not been more widely adopted for viscous flow problems is that the details of the displacement field have not been calculated in a rigorous manner. As indicated, the influence of vorticity on the displacement field is significant and fundamentally changes Darwin's result. As we shall also show, the influence of bounding surfaces must also be considered because they change how rapidly the velocity perturbation decays in the far field. The paper is structured as follows: the Stokes flow past a spherical droplet moving in an unbounded flow is described in § 2. Asymptotic expressions are then derived for fluid displacement and drift volumes in unbounded viscously dominated flows, and these results are tested against numerical simulations. In § 3, the analysis is extended to account for a planar rigid wall and partial drift volume is shown to tend to a constant value. Conclusions are drawn in § 4.

2. Fluid displacement and partial drift volume in unbounded flows

The flow $\boldsymbol{u}$ around a spherical droplet fixed in a uniform flow of speed U, expressed in spherical polar coordinates (r, θ), is related to the streamfunction Ψ (Batchelor

1967, p. 79) through

$$\boldsymbol{u} = (u_r, u_\theta) = \left(\frac{1}{r^2 \sin\theta} \frac{\partial \Psi}{\partial \theta}, -\frac{1}{r \sin\theta} \frac{\partial \Psi}{\partial r} \right). \tag{2.1}$$

The streamfunction describing uniform flow past a spherical droplet is

$$\Psi = U r^2 \sin^2\theta \left(-\frac{1}{2} + \frac{g_1 a}{r} + \frac{d_1 a^3}{r^3} \right) \tag{2.2}$$

(see Pozrikidis 1992, p. 207) where g_1 and d_1 are respectively the dimensionless strength of the Stokeslet and potential dipole which characterize the exterior flow and which are determined by λ, the ratio of the internal viscosity of the spherical droplet to the external fluid viscosity, through

$$g_1 = \frac{1}{4} \frac{3\lambda + 2}{\lambda + 1}, \quad d_1 = -\frac{1}{4} \frac{\lambda}{\lambda + 1} \left(= \tfrac{1}{2} - g_1 \right). \tag{2.3}$$

The viscous flow past an inviscid bubble and rigid sphere are determined in the limits of $\lambda \to 0, \infty$ respectively.

The displacement of fluid particles by the flow past a spherical droplet is studied analytically by developing asymptotic expressions for displacement which are valid for particles starting close to, and far from, the stagnation streamline. These results are tested numerically and applied to interpret and calculate the partial drift volume in unbounded and bounded domains.

2.1. *Fluid particle displacement for the flow around a spherical droplet*

The displacement of a fluid particle in the direction of translation of a body, X, is determined by the integrated effect of the component of the velocity perturbation parallel to the mean flow (in the x-direction) and is defined by

$$X = \int_0^t (U + u_x)\, \mathrm{d}t. \tag{2.4}$$

Fluid particles tend to a distance ρ_0 from the centreline far up- and downstream of the sphere (because of fore–aft symmetry), and this distance is related to the value of the streamfunction on the corresponding streamline through

$$\rho_0^2 = -\frac{2\Psi}{U} = r^2 \sin^2\theta \left(1 - \frac{2 g_1 a}{r} - \frac{2 d_1 a^3}{r^3} \right). \tag{2.5}$$

The displacement (2.4) resulting from the advection of a fluid particle from an angular position $\theta = \theta_i$ to downwind position θ_f may be recast, using $\mathrm{d}x = r\, \mathrm{d}\theta$, exactly as

$$X(\theta_f, \theta_i, \rho_0) = \int_{\theta_i}^{\theta_f} a r \left[\frac{g_1 r^2 (2 - \sin^2\theta) + d_1 a^2 (2 - 3\sin^2\theta)}{(r^3 - g_1 r^2 a + d_1 a^3) \sin\theta} \right] \mathrm{d}\theta. \tag{2.6}$$

Lighthill (1953) calculated analytically the displacement of fluid particles due to the inviscid flow past a sphere, and this methodology is applied here (see also Eames *et al.* 1994).

2.1.1. *Asymptotic expression for $X(\theta_f, \theta_i, \rho_0)$ far from centreline*

Far from the centreline ($\rho_0/a \gg 1$), the streamlines are essentially parallel and the radial position of a fluid particle moving a streamline, calculated from (2.5), is

$$r = \frac{\rho_0}{\sin\theta} \left(1 + \frac{g_1 a \sin\theta}{\rho_0} + \frac{g_1^2 a^2 \sin^2\theta}{2\rho_0^2} + O\left(\frac{a^3}{\rho_0^3} \right) \right). \tag{2.7}$$

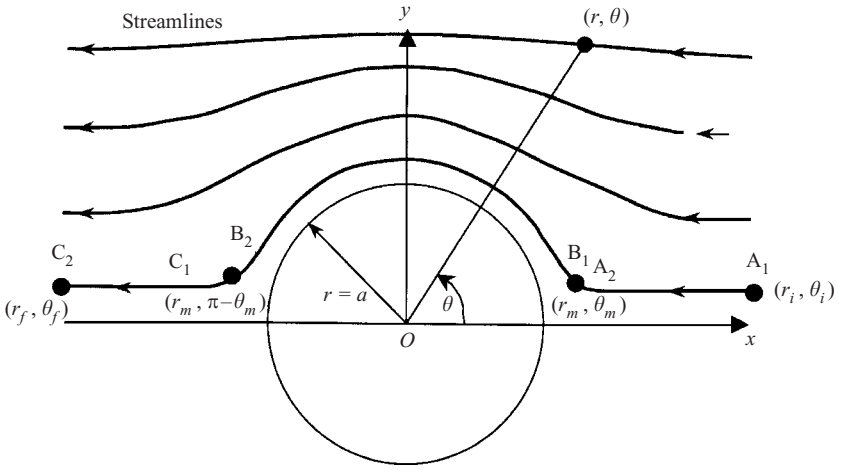

FIGURE 2. Schematic showing the notation employed to calculate asymptotic expressions for the fluid particle displacement close to the stagnation streamline.

Substituting (2.6) into (2.4), expanding the integrand in powers of $(\rho_0/a)^{-1}$ and integrating, we obtain the leading-order contribution to the displacement,

$$X(\theta_f, \theta_i, \rho_0) = \left[g_1 a \left(\cos\theta + 2\log\left(\tan\tfrac{1}{2}\theta\right)\right) + \frac{g_1^2 a^2}{\rho_0}\left[\tfrac{3}{2}\theta + \tfrac{1}{4}\sin 2\theta\right]\right]_{\theta_i}^{\theta_f}. \tag{2.8}$$

The fluid particle displacement is dominated by the strength of the Stokeslet because the potential dipole contribution decays so rapidly with distance from the droplet. As $\theta_i \to 0$ or $\theta_f \to \pi$, the displacement increases and becomes unbounded. The displacement is positive everywhere, in contrast to inviscid flows, because the streamlines (in the frame moving with the droplet) close at infinity. The largest contribution to the displacement is independent of ρ_0, and provides the bulk contribution to the partial drift volume, as we shall see later.

2.1.2. *Asymptotic expression for $X(\theta_f, \theta_i, \rho_0)$ close to the centreline*

The displacement of a fluid particle which lies initially close to the centreline ($\rho_0/a \ll 1$) is calculated by considering separately contributions from transport along the streamlines A_1A_2, B_1B_2 and C_1C_2 (see figure 2) and matching the asymptotic expansions over an intermediate region. The flow around a viscous droplet (where $0 \leqslant \lambda < \infty$) differs significantly from that around a rigid sphere (where $\lambda = \infty$) because there is slip velocity on the sphere's surface. This fundamentally changes the nature of the singularity in the centreline fluid displacement. We treat the case of a viscous spherical droplet (where λ is finite) and rigid sphere (where $\lambda = \infty$) separately.

Along A_1A_2 and C_1C_2, the streamline is described to leading order by (2.7). The contribution to displacement by a fluid particle being advected from (r_i, θ_i) to (r_m, θ_m) (from A_1 to A_2) is (from (2.4))

$$X_{A_1A_2} = \int_{r_i}^{r_m} \frac{U + u_x}{u_r}\,\mathrm{d}r = \int_{r_m}^{r_i} \frac{a(2g_1r^2 + 2d_1a^2)}{(r-a)(r^2 + 2d_1ra + 2d_1a^2)}\,\mathrm{d}r + O(\rho_0). \tag{2.9}$$

When λ is finite, the denominator in the integrand of (2.9) has only one root, $r = a$.

The first term in the expansion is

$$\left[\frac{a}{1+4d_1}\log(r-a)+\frac{2g_1(1+4d_1)-1}{2(1+4d_1)}\log(r^2+2d_1ar+2d_1a^2)\right.$$
$$\left.+\frac{2g_1(1-d_1)-(1+d_1)/(1+4d_1)}{2\left(-2d_1+d_1^2\right)^{1/2}}\log\left(\frac{r/a+d_1-\sqrt{-2d_1+d_1^2}}{r/a+d_1+\sqrt{-2d_1+d_1^2}}\right)\right]_{r_m}^{r_i}. \quad (2.10)$$

A similar expression may be calculated for $X_{C_1C_2}$, with r_i replaced by r_f.

On the streamline B_1B_2 adjacent to the droplet,

$$r=a+\frac{\rho_0^2}{(1+4d_1)a\sin^2\theta}+O\left(\rho_0^3/a^2\right). \quad (2.11)$$

The displacement contribution as a fluid particle is advected from (r_m, θ_m) to $(r_m, \pi-\theta_m)$ is

$$X_{B_1B_2}=\int_{\theta_m}^{\pi-\theta_m} a\frac{1-(g_1+3d_1)\sin^2\theta}{\frac{1}{2}(1+4d_1)\sin\theta}\,\mathrm{d}\theta+O(\rho_0). \quad (2.12)$$

On integration it yields

$$X_{B_1B_2}=-\frac{4a}{1+4d_1}\log\left(\tan\tfrac{1}{2}\theta_m\right)-\frac{4(g_1+3d_1)}{1+4d_1}a\cos\theta_m+O(\rho_0). \quad (2.13)$$

The total displacement is obtained by adding together these individual contributions,

$$X(\theta_f,\theta_i,\rho_0)=X_{A_1A_2}+X_{B_1B_2}+X_{C_1C_2}, \quad (2.14)$$

and using the matching condition (from (2.11)), $r_m=a+\rho_0^2/(1+4d_1)a\theta_m^2$. The total displacement is

$$X(\theta_f,\theta_i,\rho_0)=\left[\frac{a}{1+4d_1}\log(r/a-1)+\frac{2g_1(1+4d_1)-1}{2(1+4d_1)}\log(r^2/a^2+2d_1r/a+2d_1)\right.$$
$$\left.+\frac{2g_1(1-d_1)-(1+d_1)/(1+4d_1)}{2\left(-2d_1+d_1^2\right)^{1/2}}\log\left(\frac{r/a+d_1-\sqrt{-2d_1+d_1^2}}{r/a+d_1+\sqrt{-2d_1+d_1^2}}\right)\right]^{r_f,r_i}$$
$$-\frac{4a}{1+4d_1}\log\left(\frac{\rho_0}{2a\sqrt{1+4d_1}}\right)-\frac{4(g_1+3d_1)a}{1+4d_1}. \quad (2.15)$$

Close to the centreline, the displacement is dominated by a weak logarithmic singularity, arising from the stagnation points on the surface of the droplet. The nature of this singularity is similar to inviscid flows past a rigid body. As $\lambda\to\infty$, the strength of the potential dipole, d_1, tends to $-\frac{1}{4}$ and the asymptotic expansion described above breaks down because the azimuthal velocity tends to zero on the sphere's surface. The above calculations are repeated here for $\lambda=\infty$. In the denominator of (2.9), $r=a$ is a double root and

$$X_{A_1A_2}=\frac{14}{9}a\log\left(\frac{r_m-a}{r_i-a}\right)-\frac{2a^2}{3(r_m-a)}+\frac{2a^2}{3(r_i-a)}-\frac{1}{18}a\log\left(\frac{r_m+\frac{1}{2}a}{r_i+\frac{1}{2}a}\right)+O(\rho_0). \quad (2.16)$$

When $\lambda=\infty$, the streamline B_1B_2 is

$$r=a+\sqrt{\frac{2}{3}}\frac{\rho_0}{\sin\theta}+\frac{1}{9}\frac{\rho_0^2}{a\sin^2\theta}+O\left(\rho_0^3/a^2\right). \quad (2.17)$$

Notice the occurrence of the $O(\rho_0)$ term which arises from the no-slip condition on the surface of the sphere. The contribution from the streamline adjacent to the rigid sphere is determined by substituting (2.17) into (2.6):

$$X_{B_1B_2} = \sqrt{\frac{2}{3}}\frac{a^2}{\rho_0}(\pi - 2\theta_m) + \tfrac{28}{9}a\log\left(\tan\tfrac{1}{2}\theta_m\right) - 2a\cos\theta_m + O(\rho_0). \tag{2.18}$$

Applying the matching process described before, we find the total displacement close to the centreline is

$$X(\theta_f, \theta_i, \rho_0) = \tfrac{14}{9}a\log[(r_i/a - 1)(r_f/a - 1)] - \frac{2(r_f + r_i - 2a)a}{3(r_i - a)(r_f - a)} - \tfrac{28}{9}a\log\left(\sqrt{\frac{2}{3}}\frac{\rho_0}{2a}\right) + \sqrt{\frac{2}{3}}\frac{\pi a^2}{\rho_0} + \tfrac{1}{9}a\log\left(\tfrac{3}{2}\right) - 2a + O(\rho_0). \tag{2.19}$$

Close to the centreline, the fluid particle displacement is dominated by a ρ_0^{-1} singularity,

$$X(\theta_f, \theta_i, \rho_0) \to \sqrt{\frac{2}{3}}\frac{\pi a^2}{\rho_0}, \tag{2.20}$$

associated with the no-slip condition on the surface of the sphere.

2.2. *Partial drift volume*

The drift volume formed by an infinitely large material surface starting infinitely far in front of a steadily translating body is not well-defined. The approach adopted by Eames *et al.* (1994) is applied here, where the 'partial' drift volume formed by a material surface of (finite) radius ρ_m, starting a finite distance in front of a rigid body, is calculated. The volume formed by the deformation of a material surface, initially subtended by an angle θ_i from the x-axis and advected downstream so that it is finally subtended by an angle θ_f (see figure 3), is defined as

$$D_p(\theta_f, \theta_i, \rho_m) = \int_0^{\rho_m} X 2\pi\rho_0 \,\mathrm{d}\rho_0. \tag{2.21}$$

Insight may be obtained by applying the geometrical argument originally developed by Yih (1985) to evaluate drift volumes in potential flows. Figure 3 shows a schematic of a material surface of radius ρ_m, initially subtended by an angle θ_i, which is advected by a uniform stream past a rigid body. From the conservation of mass, the partial drift volume is related to A, the volume between the laterally displaced streamlines and their unperturbed positions, and V, the volume of the body, through

$$D_p = A - V, \tag{2.22}$$

when the body has passed through the material surface. For potential flows, A tends to $\Omega\mu/U$, as $\theta_i \to 0$, $\theta_f \to \pi$ and $\rho_m \to \infty$, where $\Omega = 2\pi$, 4π in planar and three-dimensional flows respectively and μ is the dipole moment characterizing the far-field flow. Darwin's original result is then recovered,

$$D_p = \frac{\Omega\mu}{U} - V = C_m V. \tag{2.23}$$

(Here Taylor's 1928 result $\mu = (1 + C_m)UV/\Omega$ is employed). For viscous flow past a rigid body, A is determined by ρ_m, θ_i and θ_f and does not tend to a constant value as $\rho_m/a \to \infty$.

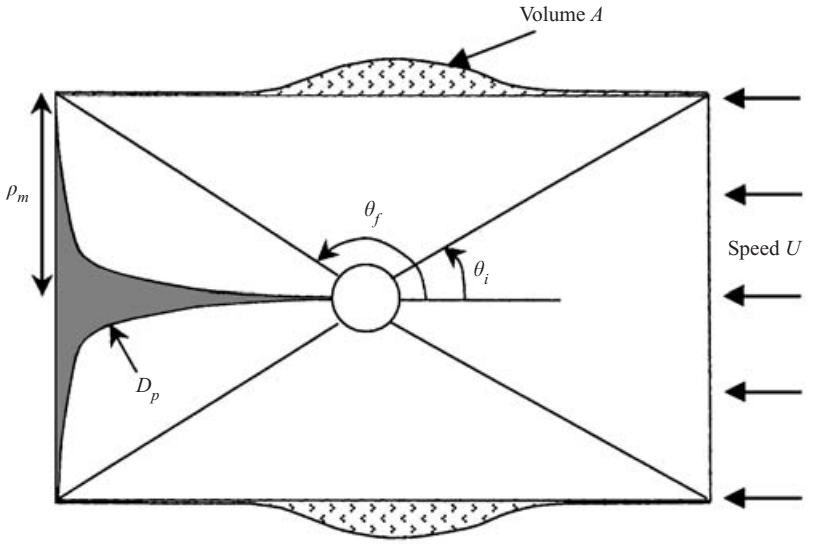

FIGURE 3. Schematic showing a geometrical argument for the evaluation of the partial drift volume.

In a viscous unbounded flow, the volume enclosed by a displacement streamline tube (of radius ρ_m) is

$$A = \int_{x_i}^{x_f} \pi\left(r^2 \sin^2\theta - \rho_m^2\right) \mathrm{d}x \tag{2.24}$$

(where r is given by (2.7)) and to leading order is evaluated to be

$$D_p = 2g_1\pi\rho_m^2 a \log\left(\frac{\tan\frac{1}{2}\theta_f}{\tan\frac{1}{2}\theta_i}\right) + 2g_1^2\pi a^2\rho_m(\theta_f - \theta_i) - V. \tag{2.25}$$

This is the viscous flow equivalent of Darwin's proposition. As $\theta_f \to 0$ and $\theta_f \to \pi$, the partial drift volume becomes unbounded. This is because the flow decays so slowly in the far field that an infinite volume of fluid is transported in the direction in which the body translates. From (2.8), we see that to leading order, $D_p \sim \pi\rho_m^2 X(\theta_f, \theta_i, \rho_m)$, because the contribution from the Stokeslet dominates the displacement field. It is important to contrast these results with the calculations of Eames *et al.* (1994) who found that the partial drift volume tends to a constant value for inviscid flows.

2.3. *Numerical results*

To test the asymptotic expressions, the fluid particle displacement was calculated numerically by integrating

$$\frac{\mathrm{d}x}{\mathrm{d}t} = u_x(x, y), \quad \frac{\mathrm{d}y}{\mathrm{d}t} = u_y(x, y), \tag{2.26}$$

subject to the initial condition $(x, y) = (x_0, y_0)$ at time $t = 0$. The initial position of the fluid particles is related to the Lagrangian variable ρ_0 through (2.5).

Figure 4 shows typical trajectories of fluid particles (in the frame moving with the mean flow) which are placed an initial distance $x_0/a = -2.5$ and 50 upstream of the sphere; the sphere moves through a distance of $100a$. In contrast to potential

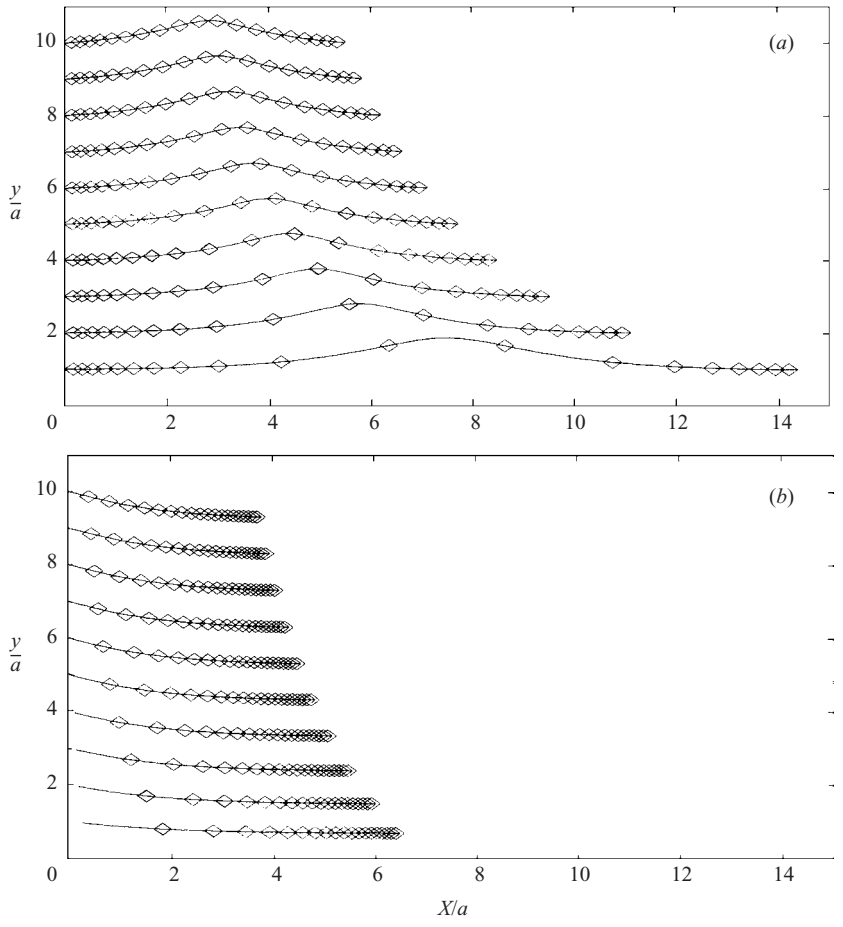

FIGURE 4. Trajectories of fluid particles which start a distance x_0 in front of the sphere where $x_0 = 50a$ and $x_0 = -2.5a$ in (a) and (b) respectively. The particles are followed for a time $100a/U$ as the sphere moves from left to right. The time difference between consecutive diamonds is $5a/U$.

flows, the fluid particles are all displaced forward by the viscous flow and there is no negative displacement or reflux (see Eames *et al.* 1994 for a comparison with the results from inviscid flows). The fluid displacement is also significantly larger than for inviscid flows, and the displacement decays slowly with ρ_0.

Figure 5 shows a comparison between asymptotic expressions and numerical results for the distortion of a material surface by a rigid sphere and inviscid bubble. The material surface starts a distance $x_0 = 50a$ in front of the sphere, and the sphere moves through a distance $2500a$. The near- and far-field expressions for displacement remain good approximations to the displacement field, giving 10% errors for both the near- and the far-field displacements, up to $O(2.0a)$ and down to $O(2.0)$, respectively. Figure 5 illustrates the change in the singularity of the centreline displacement, from $\sim -a\log(\rho_0/a)$ to $\sim a^2/\rho_0$ as λ increases. From figure 5, we see that the far-field expression (2.8) provides a reasonable prediction of the near-field behaviour for flow past a rigid sphere. This is because (2.8) is dominated by $3\pi g_1^2 a^2/2\rho_0 \approx 2.65a^2/\rho_0$, when truncated after ρ_0^{-1}, which is close to (2.20) or $X \sim 2.56a^2/\rho_0$, as $\rho_0/a \to 0$.

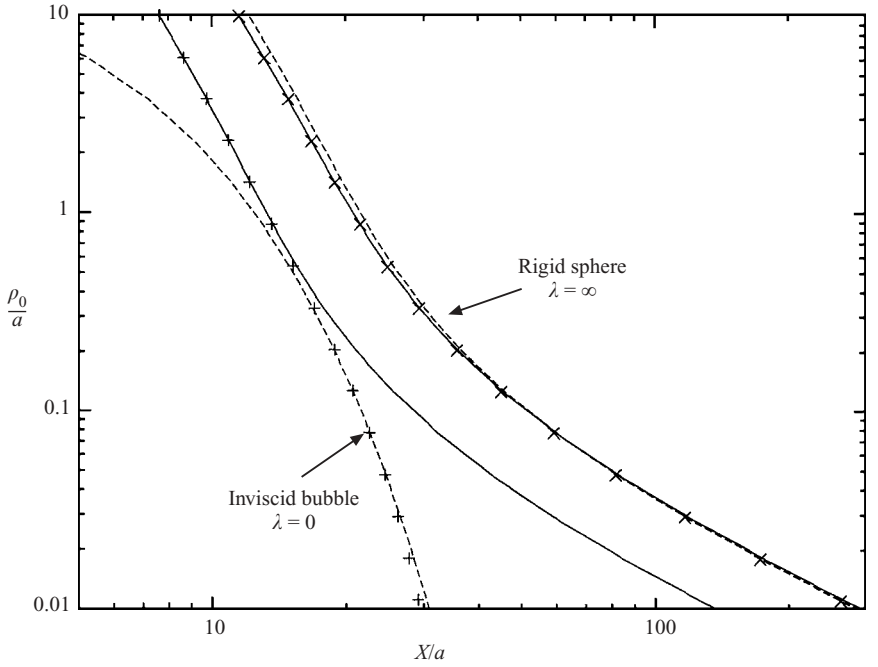

FIGURE 5. Comparison between numerical calculations of fluid particle displacement and asymptotic expressions, for a rigid sphere and inviscid bubble. The particles start a distance $x_0 = 50a$ in front of the sphere and are advected for a time $2500a/U$. Numerical results are indicated by symbols: +, an inviscid bubble ($\lambda = 0$); ×, a rigid sphere ($\lambda = \infty$). The curves describe the asymptotic results: the full curve denotes (2.8); the dashed curves denote (2.15) and (2.20) for $\lambda = 0$ and ∞ respectively.

Figure 6 shows a comparison between the asymptotic expression for the partial drift volume associated with a rigid sphere and inviscid bubble, as a function of the angular position of the material surface. Both the initial position of the material surface and its equivalent initial radius ρ_m are indicated in the figure. There appears to be relative good agreement between the asymptotic results (2.25) and the numerical results. Comparison with the far-field asymptotic result suggests that the partial drift volume scales as $X(\theta_f, \theta_i, \rho_m)\pi\rho_m^2$, with the centreline displacement making a less significant contribution to the partial drift volume.

3. Fluid displacement and partial drift volumes in bounded flows

The presence of a rigid wall (located at $x = 0$) has a significant influence on the flow, reducing the far-field flow from an $O(aU/r)$ perturbation (where r is the distance from the droplet) to $O(a^3U/r^3)$ or $O(a^2U/r^2)$ (when the body moves perpendicular or parallel to the wall respectively). Consequently fluid particles (which do not lie on the attached streamline) are displaced a finite distance. For the case of a sphere moving away from a wall, the displacement decays sufficiently rapidly from the sphere that the partial drift volume is also finite, and this is the problem we explore in more detail. The centre of the sphere is a distance $h = h_S + Ut$ (for $t > 0$) from the wall and moves away at a constant velocity U. The deformation of a material surface, which lies a distance h_L above the wall, and the corresponding partial drift volume are considered.

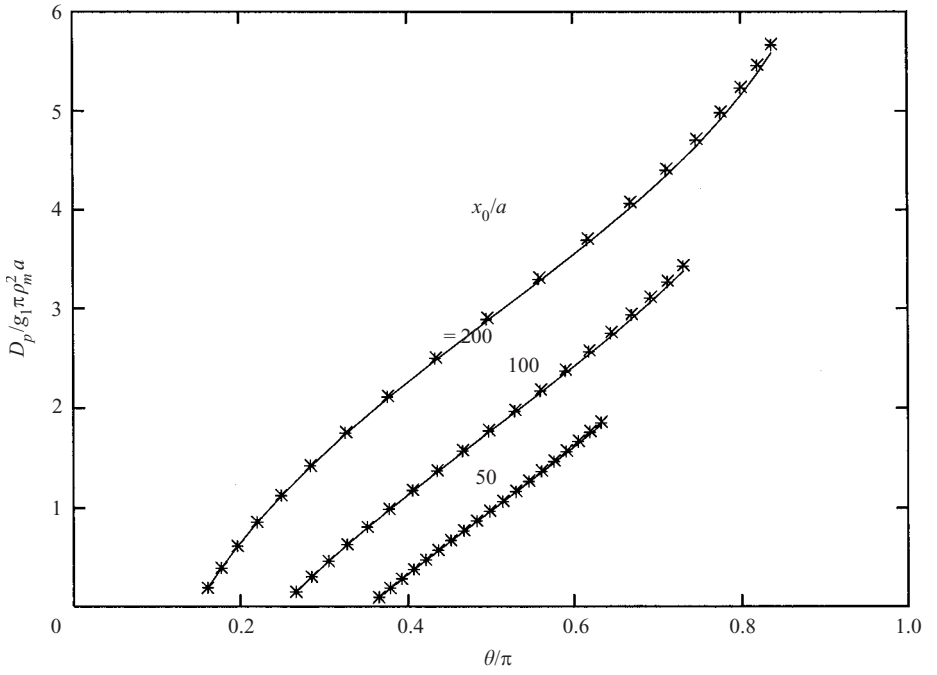

FIGURE 6. The variation of the normalized partial drift volume, $D_p/g_1\pi\rho_m^2 a$, with angular position θ (see figure 3). The drift volume is calculated by advecting a circular material surface, of initial radius $\rho_m = 100a$, past the sphere. The surface starts an initial distance x_0 in front of the sphere, and the symbols correspond to: +, an inviscid bubble ($\lambda = 0$); $\times$, a rigid sphere ($\lambda = \infty$). The initial position of the material surface, θ_i, can be determined from the intercept of the curves with the θ-axis. The curves correspond to (2.25).

The flow generated by a rigid sphere ($\lambda = \infty$) moving away from a rigid wall was calculated by Brenner (1961) as a series expressed in bispherical polar coordinates (Appendix A). When the sphere is far from the wall, the leading-order flow is described by a multipolar expansion, expressed in terms of Stokeslets and dipoles, which approximately satisfies the boundary condition on the wall and sphere. Although the kinematic boundary condition on the wall is satisfied exactly, there is a weak tangential velocity along the wall of $O(Ua^3/h^3)$ which has a negligible impact on the displacement field when h is large (see Appendix B). An indication of the accuracy of the two descriptions is the error in the kinematic boundary condition on the sphere's surface, which is discussed in Appendix B. The advantage of the multipolar approximation is that it can be applied to describe the flow generated by a droplet moving away from the wall.

3.1. *Fluid displacement away from a rigid wall*

The displacement of a fluid particle away from a wall is the integral of the velocity perturbation,

$$\lim_{t\to\infty} X(t) = \int_0^\infty u_x(h_L + X, y, t)\,\mathrm{d}t. \tag{3.1}$$

As with the inviscid flow generated by a translating body, the displacement field is only a function of the starting and finishing position of the sphere, and independent of U because the flow is reversible in time.

When the sphere is far from the wall, the flow is approximately described by a multipolar approximation:

$$u_x(x, y, t) = g_1 a U\,[S_1(x - h_S - Ut, y) - S_1(x + h_S + Ut, y) - 2hx\,D_1(x + h_S + Ut, y)] + d_1 a^3 U\,[D_1(x - h_S - Ut, y) - D_1(x + h_S + Ut, y)]. \quad (3.2)$$

(See Appendix B for the notation.) Far from the sphere and the stagnation streamline, the flow decreases sufficiently rapidly that the displacement parallel to the wall is negligible and $X \ll h_L$. The permanent displacement perpendicular to the wall is estimated to be

$$\begin{aligned}\lim_{t\to\infty} X(t) &\approx \int_0^\infty u_x(h_L, \rho_0, t)\,\mathrm{d}t \\ &= -2g_1 a \log\left(\frac{h_S - h_L + \sqrt{(h_S - h_L)^2 + \rho_0^2}}{h_S + h_L + \sqrt{(h_S + h_L)^2 + \rho_0^2}}\right) \\ &\quad + \left(g_1 a + \frac{d_1 a^3}{\rho_0^2}\right)(\cos\theta_- - \cos\theta_+) - \frac{d_1 a^3}{\rho_0^2}(\cos^3\theta_- - \cos^3\theta_+) \\ &\quad - g_1 a\left(\frac{4(h_S + h_L)^2 h_L + 2h_L\rho_0^2}{((h_S + h_L)^2 + \rho_0^2)^{\frac{3}{2}}} - \frac{4h_L^2}{2\rho_0^2}(\cos\theta_+ - \cos^3\theta_+)\right), \end{aligned} \quad (3.3)$$

where $\cos\theta_\pm = (h_S \pm h_L)/((h_S \pm h_L)^2 + \rho_0^2)^{1/2}$ and $(h_L + X, \rho_0)$ is the final position of the fluid particle. The last two terms on the right-hand side of (3.3) correspond to contributions from the image Stokeslet doublet and potential dipole required to approximately satisfy the no-slip condition on the wall, while the remaining terms (which can be identified from (2.8)) are the contributions from two separating spheres.

Asymptotic expressions for the displacement field close to the centreline are

$$\lim_{t\to\infty} X(t) \sim \begin{cases} -2g_1 a \log\left(\dfrac{h_S - h_L}{h_S + h_L}\right) - \dfrac{4h_L g_1 a}{h_S + h_L} & (h_S > h_L) \\ -4g_1 a \log\left(\dfrac{\rho_0}{2\sqrt{h_L^2 - h_S^2}}\right) - \dfrac{4h_L g_1 a}{h_S + h_L} - 2g_1 a & (h_S < h_L), \end{cases} \quad (3.4)$$

while far from the centreline,

$$\lim_{t\to\infty} X(t) \to \frac{\frac{4}{3}g_1 h_L^3 a + 2d_1 a^3 h_L}{\rho_0^3}. \quad (3.5)$$

According to the multipole approximation, the displacement $\lim_{t\to\infty} X$ is positive everywhere. When the sphere starts above the material surface ($h_S > h_L + a$), the displacement field consist of a near-field ($\rho_0 \leqslant O(h_L)$) and a far-field ($\rho_0 \geqslant O(h_L)$) component described by (3.4) and (3.5) respectively. When the sphere passes through the material surface ($h_S \leqslant h_L + a$), the displacement field consists of an inner field $\rho_0 \leqslant O(a)$ where the singularity of the displacement is $O(a^2/\rho_0)$ or $O(-a\log(a/\rho_0))$ (depending on whether the sphere is rigid or viscous) which is not captured by (3.4), an intermediate region ($a \ll \rho_0 \leqslant O(h_L)$) and a far field ($\rho_0 \geqslant O(h_L)$) described by (3.4) and (3.5) respectively. Thus, we can anticipate that (3.3) underpredicts the centreline displacement. Further, since the no-slip condition on the wall is not satisfied exactly in the multipolar approximation, it can also be anticipated that the numerical calculations of the displacement field, utilizing (3.2), would tend to over-estimate X,

far from the centreline. However, the underlying scaling, suggested by (3.5), that the displacement far from the centreline is weakly dependent on h_S, is still preserved.

3.2. *Partial drift volume*

Fluid particles are ultimately displaced away from the wall and the partial drift volume is then defined as

$$D_p = \int_0^\infty \lim_{t\to\infty} X(t) 2\pi\rho_0 \, \mathrm{d}\rho_0. \tag{3.6}$$

The partial drift volume is finite because the centreline displacement has an integrable singularity and $X \sim O(h_L^3 a/\rho_0^3)$ in the far field. (Note, in contrast to the displacement by the inviscid flow past a sphere moving away from a wall, that there is no reflux, so it is not necessary to distinguish between drift and reflux volumes, as identified by Eames, Hunt & Belcher 1996.)

An estimate of the partial drift volume using the multipolar approximation for the displacement field (3.3), gives

$$D_p = 4g_1 \pi h_L^2 a = \frac{3\lambda + 2}{\lambda + 1} \pi h_L^2 a, \tag{3.7}$$

independent of h_S and proportional to the strength of the Stokeslet characterizing the flow around the droplet. This scaling could be anticipated from (3.5), since $X \sim O(ag_1)$ over a radial distance of $O(h_L)$, from which $D_p \sim g_1 h_L^2 a$.

As described previously, the contribution from the local deformation due to the sphere moving through the material surface (in the region $\rho_0 \leqslant O(a)$) is ignored in (3.3) and so we anticipate that D_p calculated numerically is slightly larger than (3.7). When the sphere passes through the material surface ($h_S \leqslant h_L + a$) and $h_S \gg a$, the contribution from the near-field displacement field increases with h_S.

3.3. *Numerical results*

The flow generated by a rigid sphere (where $\lambda = \infty$) translating away from a rigid wall was calculated using Brenner's (1961) series expansion (Appendix A), while a multipolar approximation was applied for a viscous droplet (where $0 \leqslant \lambda < \infty$, Appendix B).

Some caveats are required regarding the numerical calculations. The convergence of Brenner's solution is slow as h increases (and round-off errors increase), so that the integration is terminated at $h = 1000a$. Comparison with the multipolar approximation suggested that this gave an error of less than 1% in calculations of the partial drift volume. Since the multipolar approximation does not satisfy exactly the boundary conditions on the sphere, marked material surfaces were chosen to start from a radial distance of $0.8a$ from the centreline (for $h_S > h_L + a$) and $0.5a$ from the sphere (for $|h_S - h_L| \leqslant a$), so that the approximation did not lead to particles entering the sphere. This region was found by trial and error so that even when $h_S = a$, the approximation could be applied. In fact this region could be significantly reduced as h_S is increased because of greater accuracy of the multipolar approximation, but for consistency this region was fixed. In the calculation of the partial drift volume, a material surface of initial radius $100a$ was considered; beyond this distance the displacement varies as $\sim h_L^3 a/\rho_0^3$, and this was exploited to calculate the additional contribution to D_p from outside this region. The radius of $100a$ was chosen to complement the truncation of the integration beyond a distance $h = 1000a$.

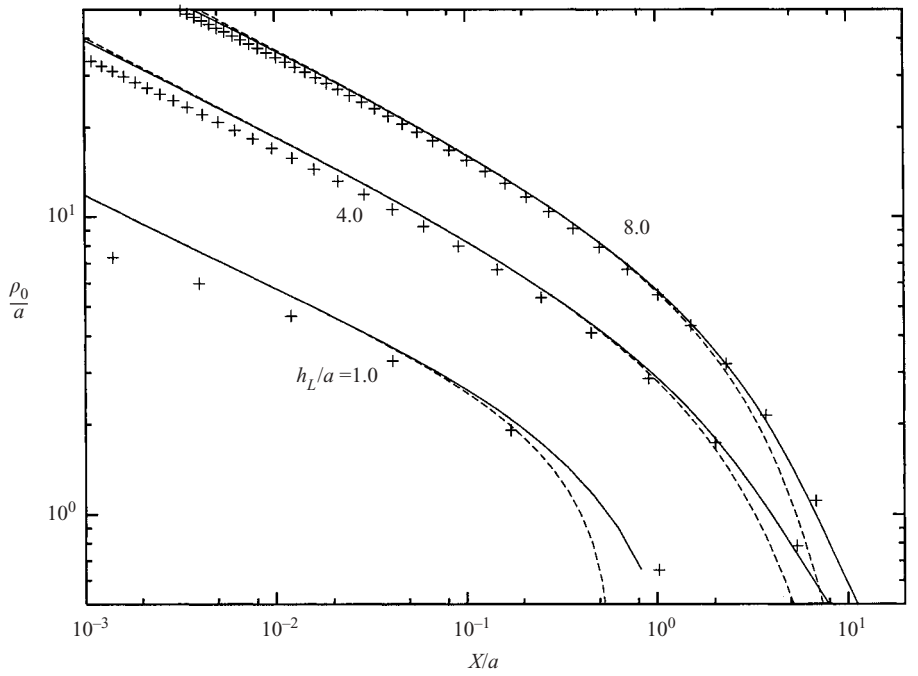

FIGURE 7. The distortion of material surfaces, initially at $h_L/a = 1, 4$ and 8, by a rigid sphere starting at $h_S/a = 4$ and moving to infinity. The numerical solution using Brenner's (1961) series is represented by +; the dashed and full curves represent numerical solutions using the multipolar approximation and (3.3). The difference between the dashed and full curves, for large ρ_0/a, is due to the fact that the integration in (3.1) is terminated at $t = (1000a - h_S)/U$.

Figure 7 shows a comparison between the distortion of a material surface for $h_S/a = 4.0$ for a rigid sphere ($\lambda = \infty$) for increasing values of h_L/a calculated using Brenner's flow description, the multipolar approximation and (3.3). Equation (3.3) underpredicts the displacement field close to the centreline because the approximation that $X \ll h_L$ breaks down. However, the displacement field is determined by the integrated effect of the velocity field, which is why the multipolar description still appears to adequately capture the distortion of the material surfaces even though this approximation is quite poor when the rigid sphere starts on the wall.

Figure 8 shows a comparison between D_p calculated numerically for a rigid sphere moving away from a rigid wall (where $g_1 = \frac{3}{4}$), and the analytical result (3.7), for a fixed value of h_S and increasing values of h_L. In figure 8, D_p is calculated using Brenner's series expansion and a multipolar approximation; both show good agreement with (3.7). When the sphere is initially above the material surface ($h_L > h_S + a$), the difference between the numerical result and (3.7) is less than 10%, and this difference decreases as h_L increases. Close to the centreline, (3.3) underpredicts X, and therefore numerical calculations for D_p in figure 8(a) lie above the analytical prediction (3.7). As h_S increases, the difference between the full numerical solution and (3.7) increases. An analysis of the results for unbounded flows indicates that this introduces terms at most of $O(h_S a^2)$, so that even as h_S increases, the main analytical result remains a good prediction of the partial drift volume. Numerical calculations of the influence of λ on $D_p/g_1\pi h_L^2 a$ (not shown here), utilizing the multipolar flow description have shown that that rigid spheres displace slightly

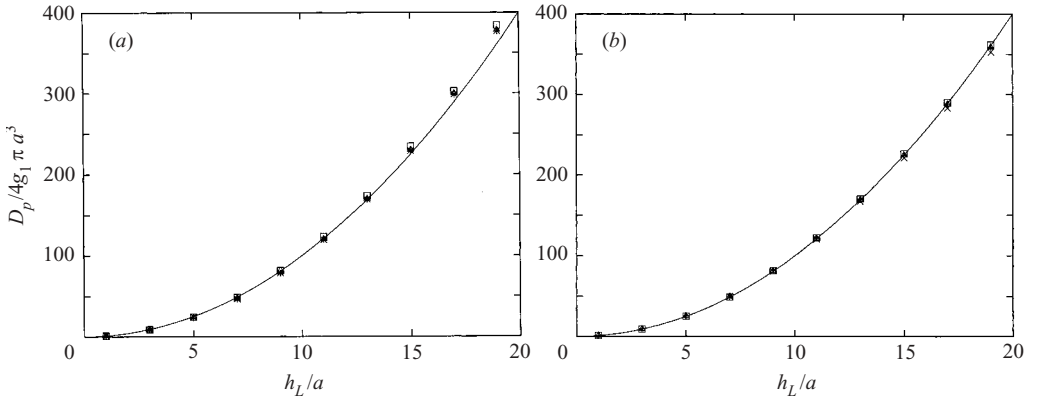

FIGURE 8. Comparison between numerical calculations of the partial drift volume, D_p, for a rigid sphere ($\lambda = \infty$, $g_1 = \frac{3}{4}$) moving away from a wall and the asymptotic result $D_p = 4g_1\pi h_L^2 a$. Brenner's series expansion for the flow is used in (*a*), while the multipolar approximation is applied in (*b*). The symbols correspond to $h_S/a = 1$ (+), 4 (×), 8 (△) and 16 (□).

more fluid away from the wall than low-viscosity droplets, than can be accounted for by (3.7). This is because (3.3) does not correctly account for displacements close to the centreline when $h_L \geqslant h_S$. From figure 8, we can conclude that the volume transported away from a rigid wall is weakly dependent on the initial starting position of the body, and depends on the initial position of the material surface.

4. Concluding remarks

In this paper we have presented a detailed study of fluid displacement by the Stokes flow past a spherical droplet in an unbounded flow and in the presence of a rigid wall. Since the transport process is dominated by the strength of the Stokeslet, g_1, these results can be readily extended to arbitrarily shaped bodies.

In an unbounded flow, the partial drift volume becomes unbounded as the droplet translates an infinite distance, or as the size of the material surface increases. All fluid particles are displaced forward because the streamlines (in the frame moving with any translating body) close at infinity, so there is no reflux field. The perturbation flow decays so slowly with distance from the body that fluid particles are displaced an infinite distance and D_p is unbounded. The presence of rigid bounding walls ensures that the velocity decays sufficiently rapidly that fluid particles (which do not lie on a stagnation streamline) are only displaced a finite distance. When a body moves parallel to a rigid wall, fluid particles are displaced a finite distance; however, there is still no reflux component to the displacement field because the streamlines (in the frame moving with the body) close at infinity. This tells us that the subtle mass conservations argument employed by Batchelor (1972) to estimate the mean settling speed of rigid spheres (and rendering certain integrals finite) requires that the flow must be bounded not just by sidewalls, but also by a top and bottom, in order that a reflux field is generated.

When a body moves perpendicular to a rigid wall, it transports a finite volume away from the wall, which is principally determined by the initial position of the material surface and rather weakly dependent on the starting position of the sphere. When a material surface is close to the wall ($h_L/a \ll 1$), the effect of viscous forces tends to inhibit the scouring action because of the no-slip condition imposed on the

wall, so that the drift volume is much smaller than for high Reynolds number and inviscid flows, where $D_p \sim 4\pi a^3 h_L/3^{\frac{3}{2}} h_S$ (Eames *et al.* 1996). But, when the material surface is initially far from the wall ($h_L/a > O(1)$), the viscous flow transports a much larger volume away from the wall (compared to inviscid flows, where $D_p \sim 2\pi a^3/3$), because the flow perturbation decays much slower with distance from the sphere. These results suggest that viscosity significantly reduces the heat transfer coefficient in pool boiling, both by reducing the rise speed of vapour bubbles and inhibiting the scouring action of the rising bubbles (Forester & Greif 1959).

The results in this paper may be applied to develop a Lagrangian coordinate system, expressed in terms of the displacement field (X, ρ_0). Such a framework is potentially useful in a number of low Reynolds number flow problems, such as dilute polymer flows past rigid bodies. In such problems, the constitutive equations are expressed in terms of a Lagrangian evolution equation describing the stretching and relaxation of polymer threads (Harlen, Rallison & Szabo 1995). An alternative approach, developed by Binous & Phillips (1999) is to follow a large number of polymer threads (modelled as beads connected by elastic threads) as they are advected past rigid bodies. The Lagrangian framework developed in this paper may provide some more insight into the stretching and alignment of polymer threads with the velocity of the body, when the polymer relaxation time is long compared to the advective timescale past the body. A future goal will be to attempt to adapt this Lagrangian formulation to this non-trivial problem.

Beyond a distance aRe^{-1} from the body, where $Re = Ua/\nu$ is the Reynolds number characterizing the flow past the body, inertial forces are important. The influence of inertia on the displacement field can be studied using an Oseen correction to the far-field flow (Lamb 1932), and applying the methodology developed in this paper. In an unbounded flow, the dependence of the partial drift volume on the radius of the material surface is much weaker (varying as $(8g_1\rho_m a^2/Re)[\tan\frac{1}{2}\theta_f - \tan\frac{1}{2}\theta_i]$), but it still tends to become unbounded as the body translates an infinite distance. Again, this is related to the slow decay of the perturbation flow and the presence of a constant volume flux downstream of the body. However, in a bounded flow, additional physical processes, such as vorticity annihilation (Hunt & Eames 2002), are present which ultimately means that the flow is irrotational far downstream. Many of these processes still need support from detailed experimental observations before a complete physical picture of the coupling between the motion of particles and its global impact on the fluid flow, interpreted through the displacement field, can be quantified.

I.E. gratefully acknowledges support through an EPSRC. Advanced Research Fellowship held at University College London, and from an EPSRC. Mathematics and Engineering Connectivity grant to undertake this work with S.D.

Appendix A

Brenner (1961) developed a series solution describing quasi-steady Stokes flow past a rigid sphere moving perpendicular to a wall, using bipolar spherical coordinates. Solutions corresponding to rigid and shear-free walls were derived by Brenner (1961), although here we discuss only the case of a rigid wall. The bipolar coordinates (ζ, η) of a point in a meridian plane are related to the Cartesian coordinates (x, y) through $x = c\sin\eta/(\cosh\zeta - \cos\eta)$ and $y = c\sinh\zeta/(\cosh\zeta - \cos\eta)$. The surface of the sphere and rigid wall correspond to $\zeta = \alpha$ and $\zeta = 0$ respectively. The centre of the sphere lies

at a distance h from the plane $x=0$, where $h=c\coth\alpha$ or $\alpha=\log(h/a+\sqrt{(h/a)^2-1})$. The streamfunction, Ψ, satisfies the biharmonic equation $\nabla^2(\nabla^2\Psi)=0$ whose general solution is

$$\Psi=\frac{1}{(\cosh\zeta-\mu)^{\frac{3}{2}}}\sum_{n=1}^{\infty}\left(a_n\cosh\left(n-\tfrac{1}{2}\right)\zeta+b_n\sinh\left(n-\tfrac{1}{2}\right)\zeta\right.$$
$$\left.+c_n\cosh\left(n+\tfrac{3}{2}\right)\zeta+d_n\sinh\left(n+\tfrac{3}{2}\right)\zeta\right)\left(\frac{P_{n-1}(\mu)-P_{n+1}(\mu)}{2n+1}\right), \quad \text{(A 1)}$$

where $\mu=\cos\eta$. Brenner (1961) derived the coefficients a_n, b_n, c_n, d_n required to satisfy the no-slip condition on the wall and sphere's surface:

$$c_n=-a_n=\frac{\sinh^4\alpha n(n+1)(2n+1)}{\sqrt{2}\left(4\sinh^2\left(n+\tfrac{1}{2}\right)\alpha-(2n+1)^2\sinh^2\alpha\right)}$$

and

$$d_n=-\left(\frac{2n-1}{2n+3}\right),\ b_n=-\frac{\sinh^2\alpha n(n+1)}{\sqrt{2}(2n+3)}\left(\frac{2\sinh(2n+1)\alpha+(2n+1)\sinh 2\alpha}{4\sinh^2\left(n+\tfrac{1}{2}\right)\alpha-(2n+1)^2\sinh^2\alpha}-1\right).$$

Appendix B

The flow past a spherical droplet moving parallel to the x-axis in an unbounded flow can be expressed in terms of a Stokeslet and potential dipole (Pozrikidis 1992, p. 202):

$$u_i(\boldsymbol{x})=g_1aUS_i(\boldsymbol{x})+d_1a^3UD_i(\boldsymbol{x}), \quad \text{(B 1)}$$

where g_1 and d_1 are given by (2.3), and $i=1,2$ correspond to the x- and y-axis respectively. The flows due to the Stokeslet and potential dipole are

$$S_i(\boldsymbol{x})=\frac{\delta_{1i}}{|\boldsymbol{x}|}+\frac{x_1x_i}{|\boldsymbol{x}|^3}, \quad D_i(\boldsymbol{x})=-\frac{\delta_{1i}}{|\boldsymbol{x}|^3}+3\frac{x_1x_i}{|\boldsymbol{x}|^5}.$$

An approximate description of the flow around a sphere moving perpendicularly to a rigid wall may be constructed by adding image singularities (described by Blake 1971) to approximately satisfy the boundary conditions on the wall. We also add an image contribution of the potential dipole to ensure that far from the wall the flow approximation in the vicinity of the droplet tends to (B 1) as $h/a\to\infty$. The approximate description of the flow generated by a sphere at $h\hat{\boldsymbol{x}}$, which is moving with speed U, is

$$u_i=g_1aU\left[S_i(\boldsymbol{x}-h\hat{\boldsymbol{x}})-S_i(\boldsymbol{x}+h\hat{\boldsymbol{x}})+2h^2D_i(\boldsymbol{x}+h\hat{\boldsymbol{x}})-2hG_i^{SD}(\boldsymbol{x}+h\hat{\boldsymbol{x}})\right]$$
$$+d_1a^3U\left[D_i(\boldsymbol{x}-h\hat{\boldsymbol{x}})-D_i(\boldsymbol{x}+h\hat{\boldsymbol{x}})\right], \quad \text{(B 2)}$$

where

$$G_i^{SD}=x_1D_i+\frac{(\delta_{1i}x_i-x_1)}{|\boldsymbol{x}|^3}.$$

The maximum error in the kinematic condition over the surface of the sphere, $E=\max\{\hat{\boldsymbol{n}}\cdot(\boldsymbol{u}-U\hat{\boldsymbol{x}})/U\}=1.5g_1(a/h)$, is plotted in figure 9 and decreases as h/a

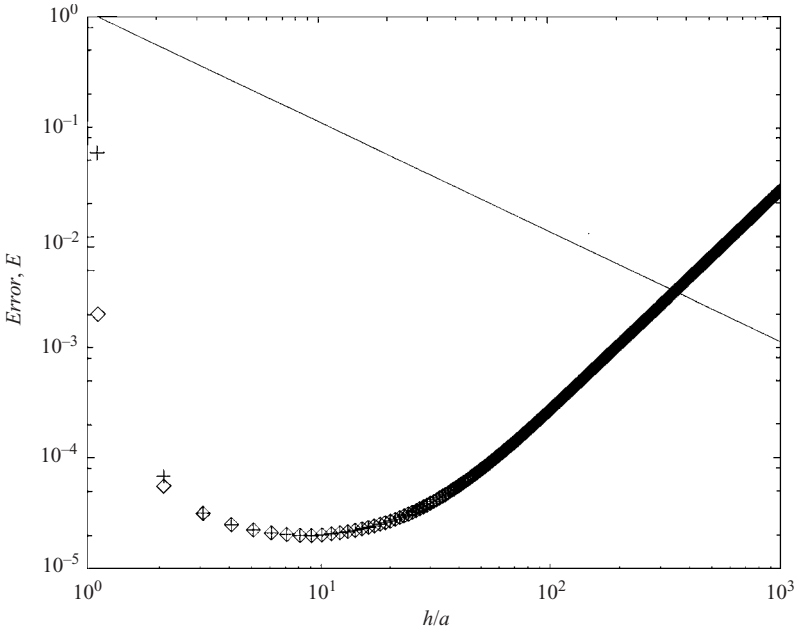

FIGURE 9. Maximum error, $E = \max\{\hat{\boldsymbol{n}} \cdot (\boldsymbol{u} - U\hat{\boldsymbol{x}})/U\}$, in the kinematic condition satisfied on the surface of the sphere, is plotted as a function of h/a. The symbols correspond to Brenner's solution, with 10 terms (+) and 30 terms (◊) evaluated in the series (A 1); the full curve corresponds to the multipolar approximation (B 2).

increases. Under this approximation, the no-slip condition is not satisfied exactly on the wall, where the slip speed is $O(Ua^3/h^3)$.

REFERENCES

BATCHELOR, G. K. 1967 *An Introduction to Fluid Dynamics*. Cambridge University Press.

BATCHELOR, G. K. 1972 Sedimentation in a dilute dispersion of spheres. *J. Fluid Mech.* **52**, 245–268.

BENJAMIN, T. B. 1986 Note on added mass and drift. *J. Fluid Mech.* **169**, 251–256.

BETZ, A. 1925 A method for the direct determination of profile drag. *Z. Flugtechn. Motorluftschiffahrt*. **16**, 42 (in German).

BINOUS, H. & PHILLIPS, R. J. 1999 Dynamics simulation of one or two particles sedimenting in viscoelastic suspensions of FENE dumbbells. *J. Non-Newtonian Fluid Mech.* **83**, 93–130.

BLAKE, J. R. 1971 A note on the image system for a Stokeslet in a no-slip boundary. *Proc. Camb. Phil. Soc.* **70**, 303–310.

BRENNER, H. 1961 The slow motion of sphere through a viscous fluid towards a plane surface. *Chem. Engng Sci.* **16**, 242–251.

BUSH, J. W. M. & EAMES, I. 1998 Fluid displacement by two-dimensional bubbles rising in a thin gap. *Intl J. Multiphase Flow* **24**, 411–430.

DARWIN, C. 1953 A note on hydrodynamics. *Proc. Camb. Phil. Soc.* **49**, 342–352.

EAMES, I., BELCHER, S. E. & HUNT, J. C. R. 1994 Drift, partial drift and Darwin's proposition. *J. Fluid Mech.* **275**, 201–223.

EAMES, I. & DALZIEL, S. B. 2000 Resuspension of dust by the flow past a sphere moving near a wall. *J. Fluid Mech.* **403**, 77–102.

EAMES, I. & FLOR, J.-B. 1998 Fluid transport by dipolar vortices. *Dyn. Atmos. Oceans* **28**, 93–105.

EAMES, I., HUNT, J. C. R. & BELCHER, S. E. 1996 Displacement of inviscid fluid by a sphere moving away from a wall. *J. Fluid Mech.* **324**, 333–353.

Forster, D. E. & Grief, R. 1959 Heat transfer to a boiling-liquid mechanism and correlation. *Trans. ASME*: *J. Heat Transfer* **81**, 43–53.

Griffith, R. W. 1986 Particle motions induced by spherical convective elements in Stokes flow. *J. Fluid Mech.* **166**, 139–159.

Harlen, O. G., Rallison, J. M. & Szabo, P. 1995 A split Lagrangian-Eulerian method for simulating transient viscoelastic flows. *J. Non-Newtonian Fluid Mech.* **60**, 81–104.

Hunt, J. C. R. 1973 A theory of turbulent flow around two-dimensional bluff bodies. *J. Fluid Mech.* **61**, 625–706.

Hunt, J. C. R. & Eames, I. 2002 The disappearance of laminar and turbulent wakes in complex flows. *J. Fluid Mech.* **457**, 111–132.

Kowe, R., Hunt, J. C. R., Hunt, A., Couet, B. & Bradbury, L. J. S. 1988 The effects of bubbles on the volume fluxes and the presence of pressure gradients in unsteady and non-uniform flow of liquids. *Intl J. Multiphase Flow* **14**, 587–606.

Lamb, H. 1932 *Hydrodynamics.* Cambridge University Press.

Lighthill, M. J. 1956 Drift. *J. Fluid Mech.* **1**, 31–54.

Magnaudet, J. & Eames, I. 2000 The motion of high-Reynolds-number bubbles in homogenous flows. *Annu. Rev. Fluid Mech.* **32**, 659–708.

Owen, P. R. 1980 Sediment transport. Unpublished Trieste Lectures. [Available from I.E.]

Pozrikidis, C. 1992 *Boundary Integral and Singularity Methods for Linearised Viscous Flows.* Cambridge University Press.

Taylor, G. I. 1928 The energy of a body moving in an infinite fluid, with application to airships. *Proc. R. Soc. Lond.* A **70**, 13–31.

Yih, C. S. 1985 New derivations of Darwin's Theorem. *J. Fluid Mech.* **152**, 163–172.